Electronic Supplementary Information for PCCP article:

Phase changes of the water hexamer and octamer in gas phase and adsorbed on polycyclic aromatic hydrocarbons

Luiz Fernando L. Oliveira, Jérôme Cuny, Maxime Morinière, Léo Dontot, Aude Simon, Fernand Spiegelman and Mathias Rapacioli

In the following supplementary information, we present additional pictures to illustrate the convergence of the heat capacity curves with the length of the simulation, the effect of the choice of the DFTB Mulliken or CM3 charges, as well as the effect of freezing the PAH intramolecular degrees of freedom. Molecular representations of the relevant cluster structures discussed in the article are also provided as well as a description of the multiple histogram method applied to the calculation of the heat capacity curves.

Contents

1 Convergency of the heat capacity curve for water hexamer

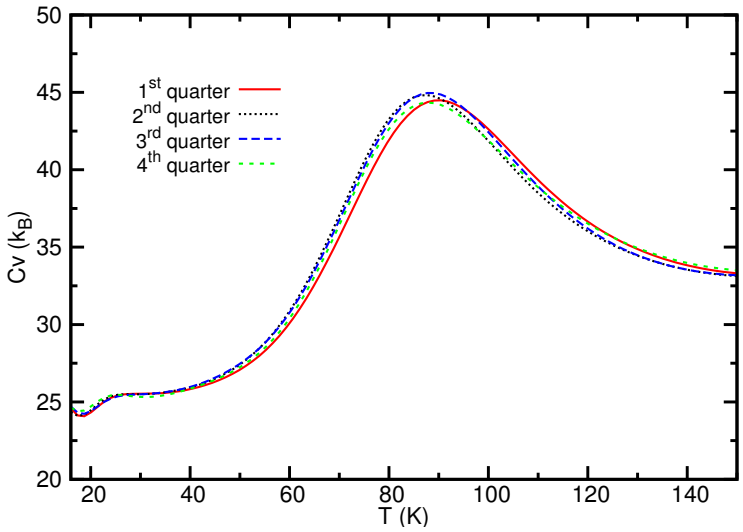

Figure 1: Comparison of the heat capacity curves for $(H_2O)_6$ computed from the first, second, third and fourth quarter of the MDPT simulation.

2 Comparison of heat capacity curves obtained with different atomic charges

2.1 Water hexamer

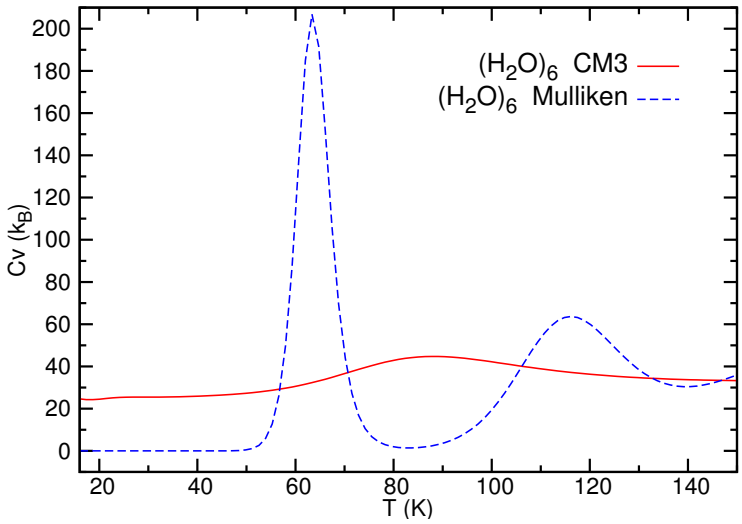

Figure 2: Heat capacity curves for $(H_2O)_6$ obtained from MDPT simulation with SCC-DFTB using CM3 and Mulliken atomic charges.

2.2 Water octamer

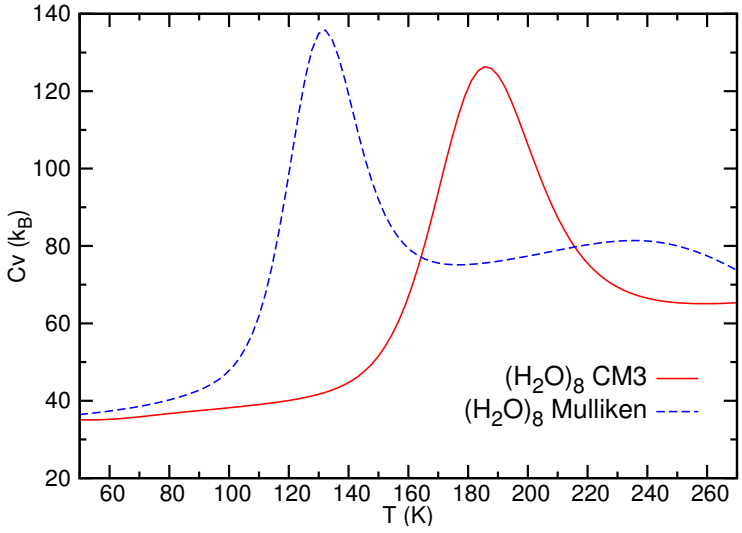

Figure 3: Heat capacity curves for $(H_2O)_8$ obtained from MDPT simulation with SCC-DFTB using CM3 and Mulliken atomic charges.

3 Effect of freezing PAH intramolecular degrees of freedom on the heat capacity curves

3.1 Water octamer on coronene

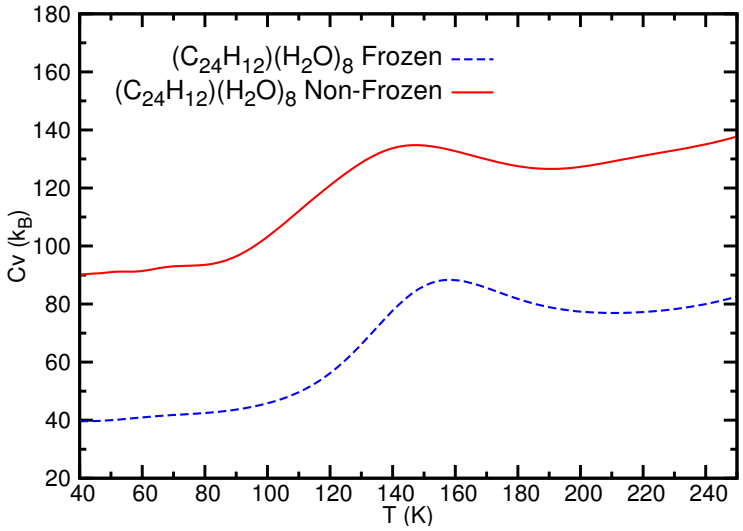

Figure 4: Heat capacity curves for the water octamer adsorbed on coronene. Comparison for frozen and non-frozen coordinates of the PAH.

3.2 Water octamer on circumcoronene

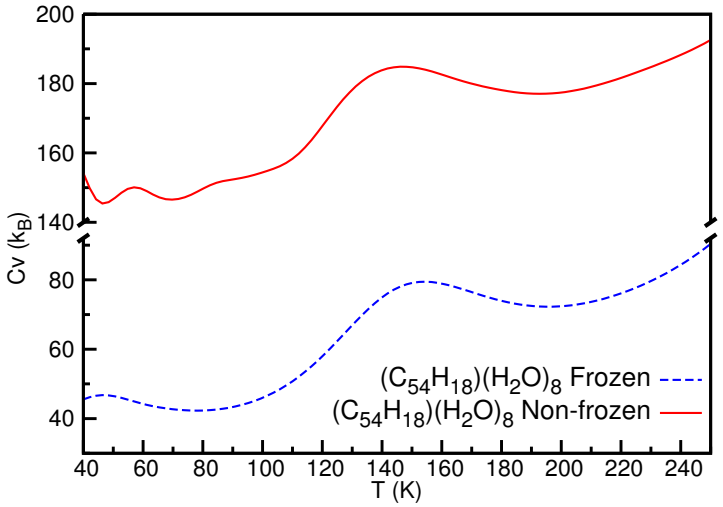

Figure 5: Heat capacity curves for water octamer adsorbed on circumcoronene. Comparison for frozen and non-frozen coordinates of the PAH.

4 Representation of relevant isomers

4.1 Water hexamer

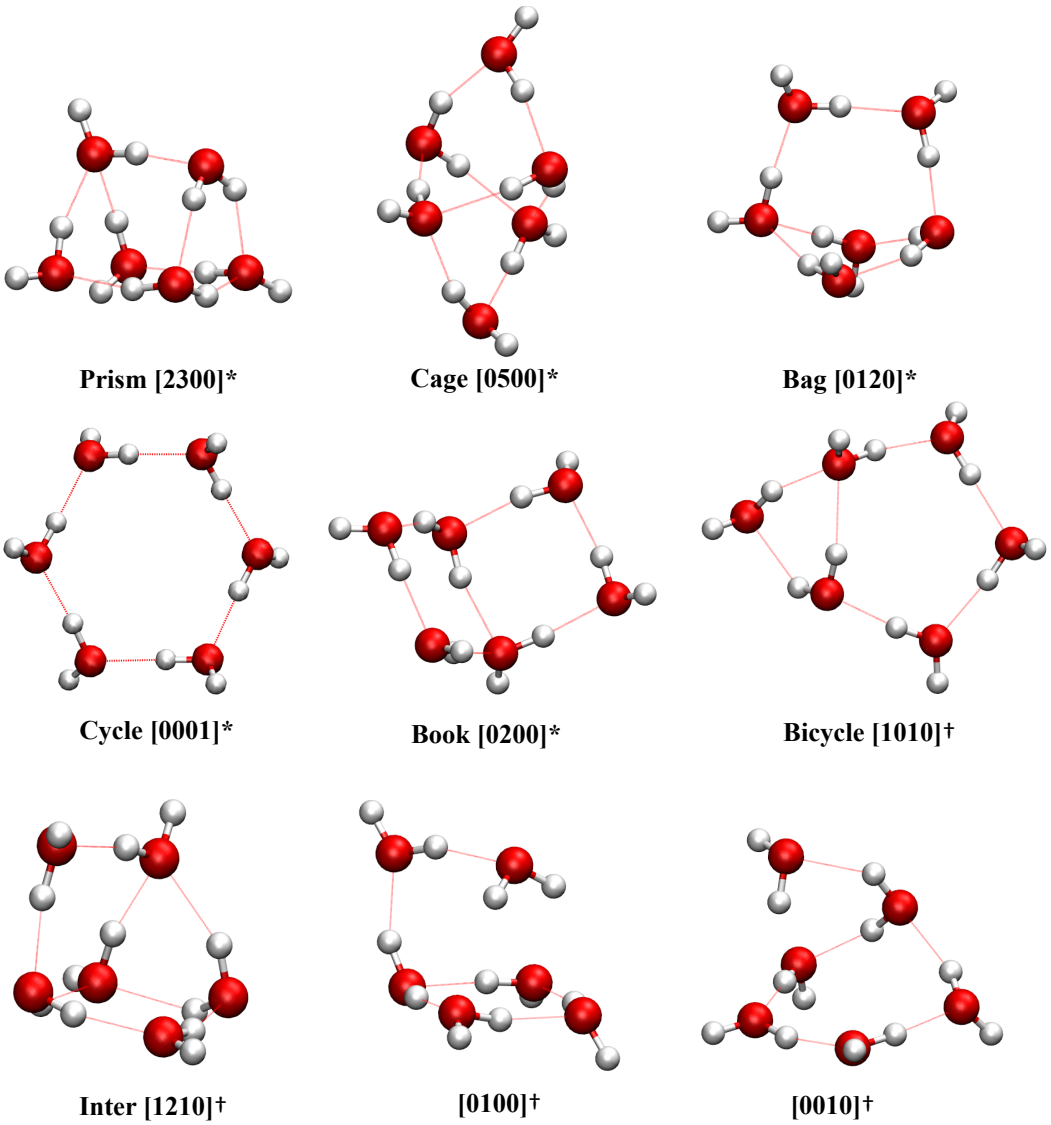

Figure 6: Molecular representation of the $(H_2O)_6$ cluster structures discussed in the manuscript. Structures marked with a * symbol are optimized geometries (energies reported on table 1). Structures marked with a † symbol correspond to snapshots extracted from the MDPT simulations, not stable with respect to optimization.

4.2 Water hexamer on coronene

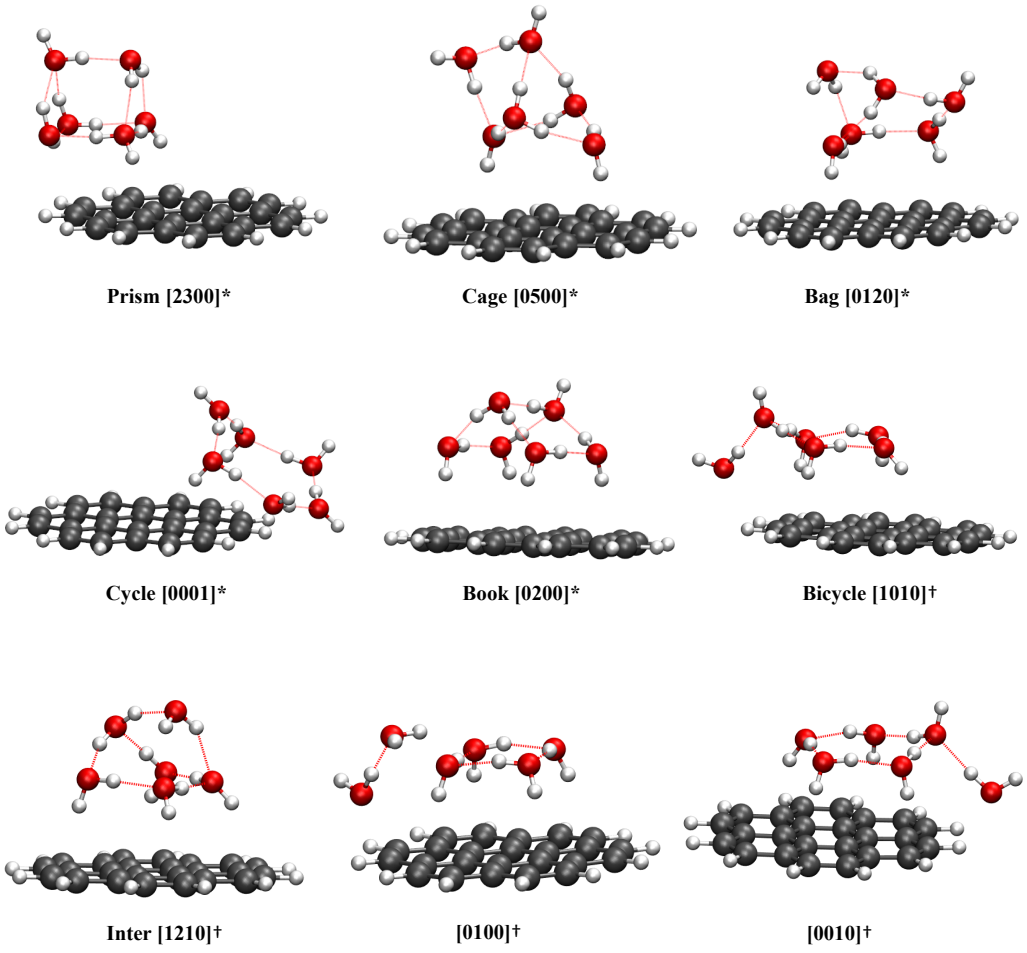

Figure 7: Molecular representation of the $(C_{24}H_{12})(H_2O)_6$ cluster structures discussed in the manuscript. Structures marked with a * symbol are optimized geometries (energies reported on table 1). Structures marked with a † symbol correspond to snapshots extracted from the MDPT simulations, not stable with respect to optimization.

4.3 Water hexamer on circumcoronene

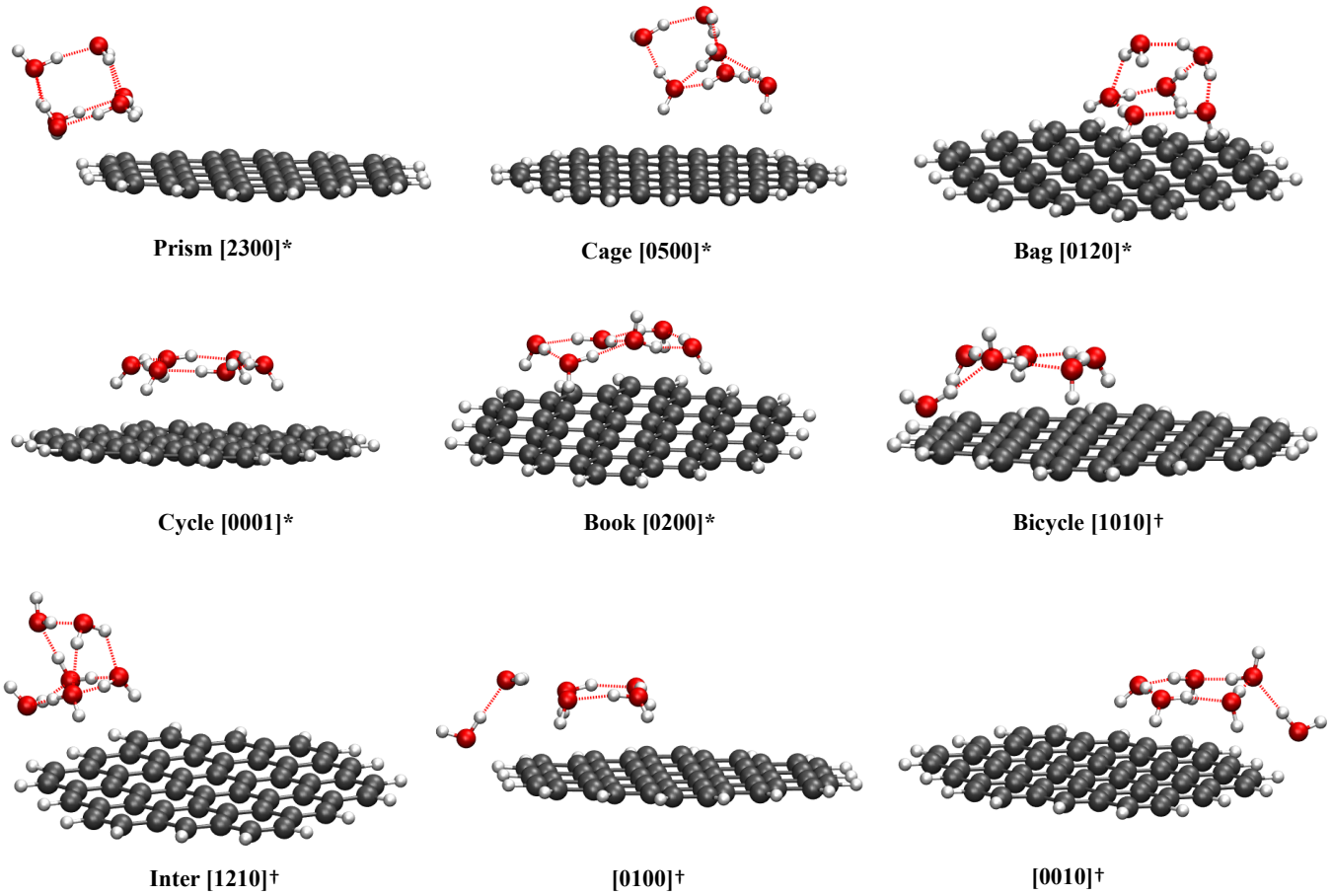

Figure 8: Molecular representation of the $(C_{54}H_{18})(H_2O)_6$ cluster structures discussed in the manuscript. Structures marked with a * symbol are optimized geometries (energies reported on table 1). Structures marked with a † symbol correspond to snapshots extracted from the MDPT simulations, not stable with respect to optimization.

4.4 Water octamer

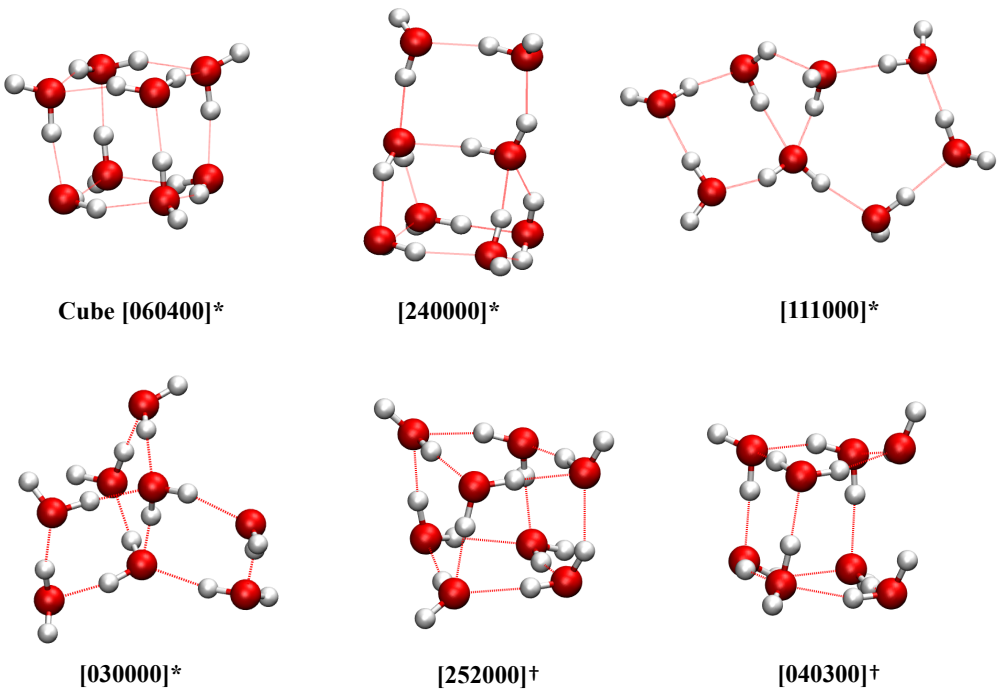

Figure 9: Molecular representation of the $(H_2O)_8$ cluster structures discussed in the manuscript. Structures marked with a * symbol are optimized geometries (energies reported on table 1). Structures marked with a † symbol correspond to snapshots extracted from the MDPT simulations, not stable with respect to optimization.

4.5 Water octamer on coronene

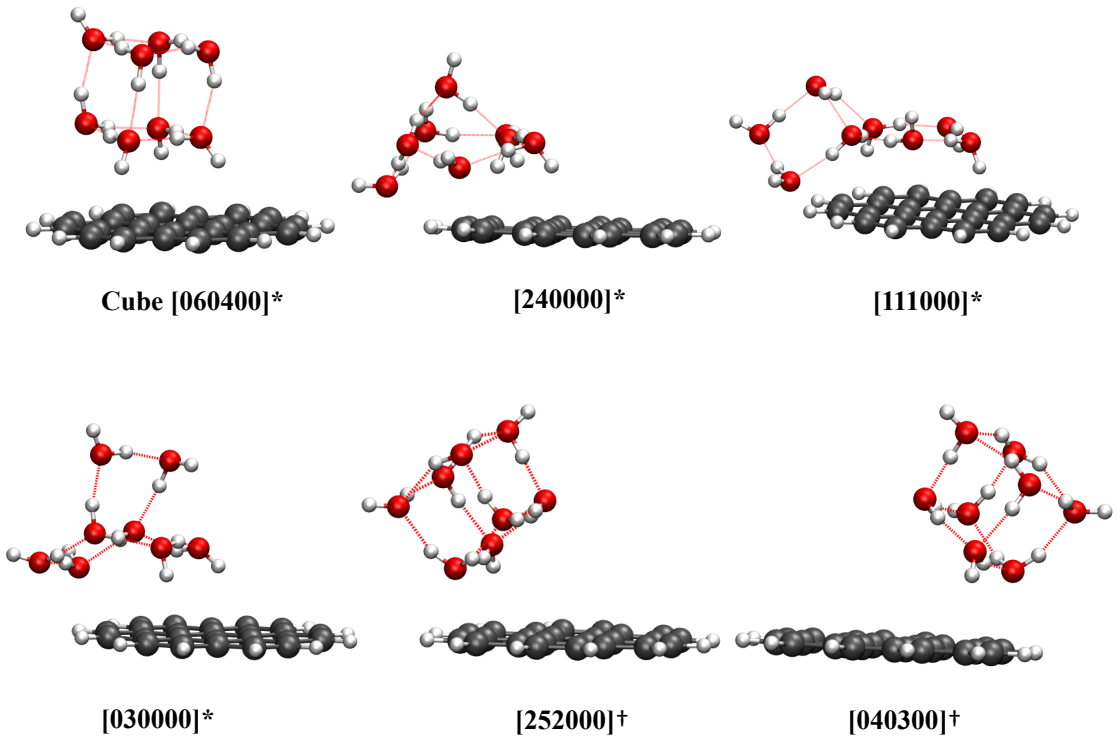

Figure 10: Molecular representation of the $(C_{24}H_{12})(H_2O)_8$ cluster structures discussed in the manuscript. Structures marked with a * symbol are optimized geometries (energies reported on table 1). Structures marked with a † symbol correspond to snapshots extracted from the MDPT simulations, not stable with respect to optimization.

4.6 Water octamer on circumcoronene

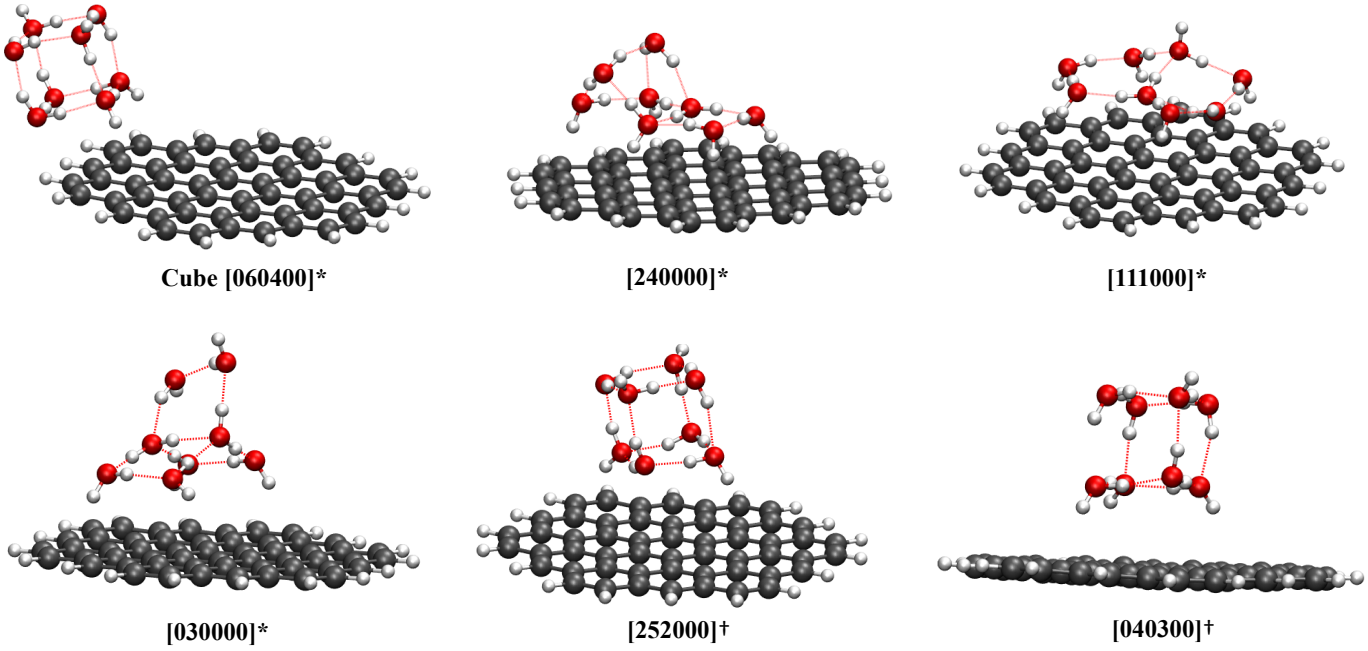

Figure 11: Molecular representation of the $(C_{54}H_{18})(H_2O)_8$ cluster structures discussed in the manuscript. Structures marked with a * symbol are optimized geometries (energies reported on table 1). Structures marked with a † symbol correspond to snapshots extracted from the MDPT simulations, not stable with respect to optimization.

5 Multiple histogram method applied to the calculation of heat capacity curves

We remind here briefly the basic equations of the multiple histogram apporach used to compute heat capacity from a set of (MD ot MC) at different temperatures T_i (more information can be found in Labastie and Whetten, PRL, 65, 1567, 1990). The interval of configurational energies visited in all simulations is divided into small intervals of energy Δ. Histograms are constructed by calculated n_{ij} as the times a value of energy V_j occurs for a the simulation at temperature T_i. Assuming ergodicity is reached, one should obtain :

$$\frac{S_j}{k_B} = (-\alpha_i + \beta_i V_j + \ln n_{ij})$$

with

$$\alpha_i = \ln\left(\sum_i n_{ij}\right) - \ln Z_i$$

where S_j is the microcanonical enthropy, Z_i the canonical partition function and $\beta_i = \frac{1}{k_B T_i}$. The following error function is introduced

$$\sum_{ij} n_{ij}\left(\frac{S_j}{k_B} + \alpha_i - \beta_i V_j - \ln n_{ij}\right)^2$$

and minimized with respect to the unknown variables α_j and S_j. This gives a system of linear equation which is solved to obtain the values of α_j. Thermodynamical properties are then derived as follows :

$$S_j = k_B \left(\frac{\sum_i n_{ij}(\ln n_{ij} + \beta_i V_j) - \sum_i n_{ij}\alpha_i}{\sum_i n_{ij}} \right)$$

$$Z(T) = \sum_j \left(S_j - \frac{V_j}{k_B T} \right).$$

$$\langle V \rangle = U = \frac{\sum_j \exp\left(S_j - \frac{V_j}{k_B T}\right) V_j}{Z}.$$

$$\langle V^2 \rangle = \frac{\sum_j \exp\left(S_j - \frac{V_j}{k_B T}\right) V_j^2}{Z}.$$

and finally the configurational contribution to the heat capacity :

$$C_v(T) = \frac{\partial U}{\partial T} = \frac{1}{k_B T^2}(\langle V^2 \rangle - \langle V \rangle^2).$$